

Chapter2

Fundamentals of VCSEL and Febry-Perot Resonator

2.1 Introduction to VCSELs^[25-27]

What is VCSEL? It is a contracted name of vertical cavity surface emitting laser and it is a kind of semiconductor laser. What's the advantage of VCSEL? What's the application of VCSEL? Before talking about these, let's review the history of the semiconductor laser.

History overview

More than forty years have been passed since the solid-state ruby laser and the He-Ne gas laser were successfully made in 1960. It was from that time, more efforts have been put on the research of laser, especially the possibility of lasing in semiconductor laser. In 1962, first stimulated emission in semiconductor laser was reported by several groups. Then, the research of the semiconductor laser never stop until now, and the related products, such as optical disc players, laser printers, and fiber communication links, have played an important role in our daily life. However, the conventional used semiconductor laser, edge emitting laser (EEL), as shown in Fig 2.1(a), still has some problems, e.g. , the initial probe test of such devices is impossible before separating into chips, the monolithic integration of lasers into an optical circuit is limited due to the finite cavity length, and so on. In 1977, K. Iga at the Tokyo Institute of Technology, Tokyo, Japan suggested a vertical cavity surface emitting laser for the purpose of overcoming such difficulties as mentioned above^[28]. As the name suggests, VCSEL emission occurs perpendicular, rather than parallel, to the wafer surface. The cavity is formed by two surfaces of an epitaxial layer, and light output is taken vertical from one of the mirror surfaces, as depicted in Fig 2.1(b). According to the suggested laser structure, many novel advantages could be done if VCSEL is realized.

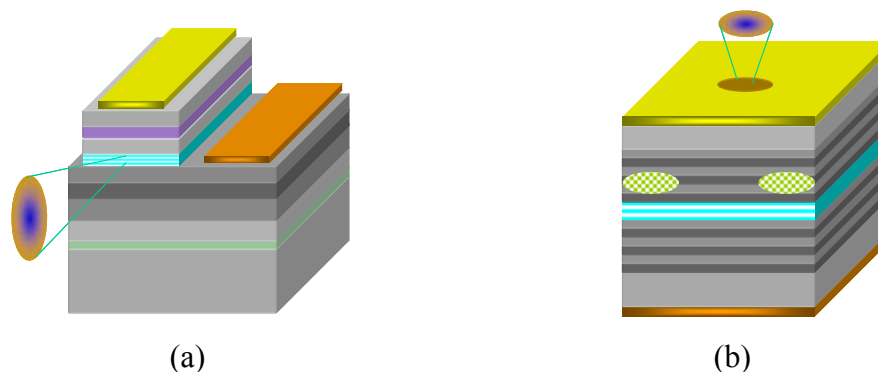


Figure 2.1 Schematic diagram of (a) an EEL and (b) a VCSEL.

The advantages of VCSEL stated by Iga are as follows [28]. (1) The laser device is fabricated by a fully monolithic process. (2) A densely packed two-dimensional laser array could be fabricated. (3) The initial probe test could be performed before separation into chips. (4) Dynamic single longitudinal mode operation is expected because of its large mode spacing. (5) It is possible to vertically stack multithin-film functional optical devices on to the VCSEL. (6) A narrow circuit beam is achievable. These benefits of VCSEL encourage the researchers to devote themselves to speeding up the development of VCSEL. In 1979, Iga demonstrated first VCSEL used 1.3 μm -wavelength GaInAsP/InP material for the active region. In 1984, they made a room temperature pulsed operation GaAs-based device, and the first room temperature continuous wave (CW) operation GaAs-based VCSEL was fabricated in 1987. Until now, Iga has done a lot of research and improvement on VCSEL. It is worth to say, his outstanding contributions on VCSEL earn him the name of “Father of VCSEL”. So far, GaAs-based device have been extensively studied and some of the 0.98, 0.85, and 0.78 μm wavelength devices are now commercialized into optical systems. Besides, the technique of 1.3 and 1.5 μm devices has already set up. In the mean while, green-blue-ultraviolet device research has been started. It is believed that the commercial products with green-blur-ultraviolet VCSEL will come out in no more future.

Typical structure of VCSEL

Typical structure of VCSEL includes central active region and the top and bottom high reflecting mirror, as shown in Fig 2.2. Besides, the high reflecting mirror is usually in the form of distributed Bragg reflectors (DBRs), composed of high and low reflection index material quarter wavelength stack, as shown in Fig 2.2. The light is amplified in the microcavity and emission out in the vertical direction. The entirely operation mechanism of VCSEL will be discussed later in section 2.5, and the theory of DBRs will also be reported in section 2.2.

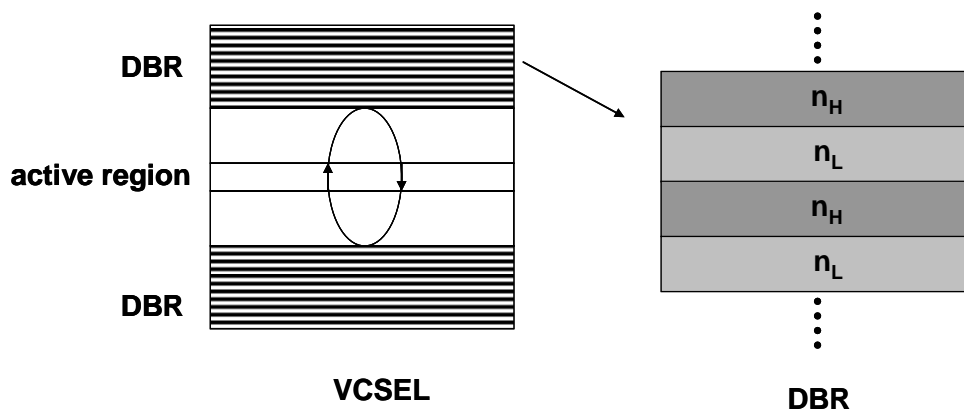


Figure 2.2 Typical structures of VCSEL and DBRs.

Advantages of VCSEL

In the past, the semiconductor laser market was filled with the product which applied the EEL, especially in optical storage devices (780nm lasers for CDs and 650nm lasers for DVDs). Recent, the semiconductor laser market has been shared by the VCSEL, due to the demand of the optical data link. Besides, the development of VCSEL grew up vary quickly these years, and more advantages of VCSEL start to surface. These advantages are as follows.

Technical advantages:

- (1) Vertical emission from the substrate with circular beam is easy to couple to optical fibers.
- (2) Low threshold and high driving current operation is possible.
- (3) Large relaxation frequency provides high speed modulation capability.
- (4) Single mode operation is possible, and wavelength and threshold are relatively insensitive against temperature variation
- (5) Long device lifetime and high power-conversion efficiency.

Manufacturing and cost advantages:

- (1) Smaller size of laser devices can lower the cost of the wafer.
- (2) The initial probe test can be performed before separating devices into discrete chips.
- (3) Easy bonding and mounting, cheap module and package cost.
- (4) Densely packed and precisely arranged two-dimensional laser arrays can be performed.
- (5) It is possible to vertically stack multithin-film functional optical devices on to the VCSEL.

Applications of VCSEL

The application of VCSEL is mainly on optical data transmission, including optical interconnects, parallel data links, and so on. The 1300nm and 1550nm long wavelength VCSEL should be useful for silica-based fiber links, providing ultimate transmission capability by taking advantage of single wavelength operation and massively parallel integration. The 650nm VCSEL is useful for short-distance data links by using 1mm diameter low loss plastic fibers. Moreover, blue to UV VCSEL should be useful in the high density data storage. Now, more and more applications of VCSEL are under development, such as compact disc optical pickup modules, printing heads, optical scanners, optical displays, projection systems, and optical sensor. It is believed that those products will be made sooner or later.

2.2 The Theory of DBRs

The DBRs are a simplest kind of periodic structure, which is made up of a number of quarter-wave layers with alternately high- and low- index materials. Therefore, it's necessary to know the theory of quarter-wave layer before discussing the DBRs.

Quarter-wave layer ^[29-30]

Consider the simple case of a transparent plate of dielectric material having a thickness d and refractive index n_f , as shown in Fig 2.3. Suppose that the film is nonabsorbing and that the amplitude-reflection coefficients at the interfaces are so low that only the first two reflected beams (both having undergone only one reflection) need be considered. The reflected rays are parallel on leaving the film and will interference at image plane.

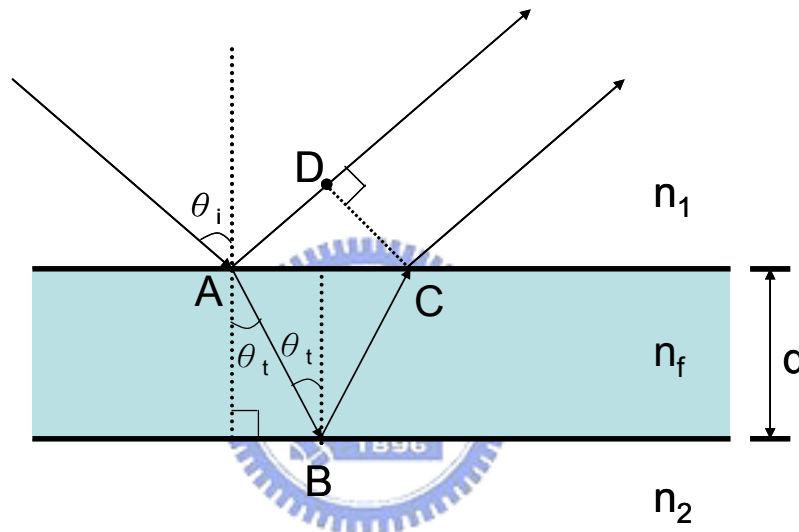


Figure 2.3 Schematic draw of the light reflected from the top and bottom of the thin film.

The optical path difference (P) for the first two reflected beam is given by

$$P = n_f[(\overline{AB}) + (\overline{BC})] - n_i(\overline{AD}) \quad (2.1)$$

and since

$$(\overline{AB}) = (\overline{BC}) = d/\cos \theta \quad (2.2)$$

$$P = \frac{2n_f d}{\cos \theta} - n_i(\overline{AD}) \quad (2.3)$$

also

$$(\overline{AD}) = (\overline{AC}) \sin \theta \quad (2.4)$$

Using Snell's Law

$$(\overline{AD}) = (\overline{AC}) \frac{n_f}{n_i} \sin \theta \quad (2.5)$$

$$(\overline{AC}) = 2d \tan \theta \quad (2.6)$$

The expression for P now becomes
$$P = \frac{2n_f d}{\cos \theta} (1 - \sin^2 \theta) \quad (2.7)$$

or finally
$$P = 2n_f d \cos \theta \quad (2.8)$$

The corresponding phase difference (δ) associated with the optical path length difference is then just the product of the free-space propagation number and P, that is, $K_0 P$. If the film is immersed in a single medium, the index of refraction can simply be written as $n_1 = n_2 = n$. It is noted that no matter n_f is greater or smaller than n , there will be a relative phase shift π radians.

Therefore,
$$d \cos \theta = (2m + 1) \frac{\lambda_f}{4} \quad (2.9)$$

or
$$\delta = \frac{4\pi n_f}{\lambda_0} (n_f^2 - n^2 \sin^2 \theta)^2 \pm \pi \quad (2.10)$$

The interference maximum of reflected light is established when $\delta = 2m\pi$, in other words, an even multiple of π . In that case Eq. (2.9) can be rearranged to yield

[maxima]
$$d \cos \theta = (2m + 1) \frac{\lambda_0}{4n_f} \quad (m = 0, 1, 2, \dots) \quad (2.11)$$

The interference maximum of reflected light is established when $\delta = (2m \pm 1)\pi$, in other words, an odd multiple of π . In that case Eq. (2.9) can be rearranged to yield

[minima]
$$d \cos \theta = 2m \frac{\lambda_0}{4n_f} \quad (m = 0, 1, 2, \dots) \quad (2.12)$$

Therefore, for a normal incident light into thin film, the interference maximum of reflected light is established when $d = \lambda_0 / 4n_f$ (at $m=0$). Based on the theory, a periodic structure of alternately high- and low- index quarter-wave layer is useful to be a good reflecting mirror. This periodic structure is also called Distributed Bragg Reflectors (DBRs).

Distributed Bragg Reflectors (DBRs) [25-26][31-34]

DBRs serve as high reflecting mirror in numerous optoelectronic and photonic devices such as VCSEL. There are many methods to analyze and design DBRs, and the matrix method is one of the popular one. The calculations of DBRs are entirely described in many optics books, and the derivation is a little too long to write in this thesis. Hence, we put it in simple to understand DBRs. Consider a distributed Bragg reflector consisting of m pairs of two dielectric, lossless materials with high- and low- refractive index n_H and n_L , as shown in Fig 2.4. The thickness of the two layers is assumed to be a quarter wave, that is, $L_1 = \lambda_B/4n_H$ and $L_2 = \lambda_B/4n_L$, where the λ_B is the Bragg wavelength.

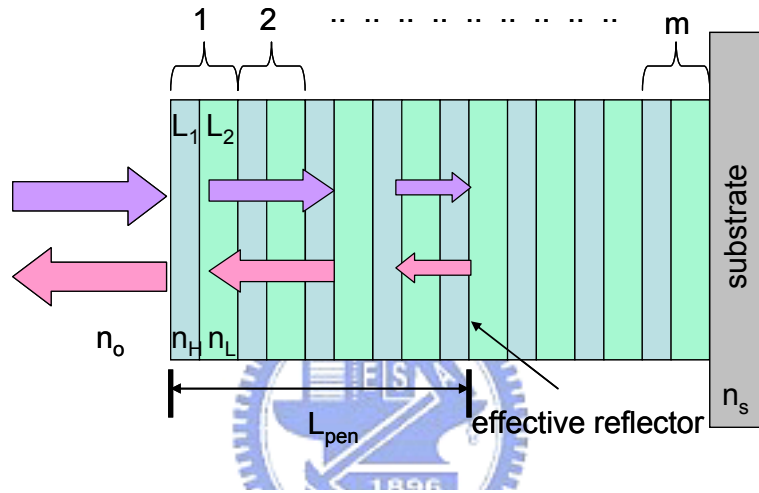


Figure 2.4 Schematic diagram of DBRs.

Multiple reflections at the interface of the DBR and constructive interference of the multiple reflected waves increase the reflectivity with increasing number of pairs. The reflectivity has a maximum at the Bragg wavelength λ_B . The reflectivity of a DBR with m quarter wave pairs at the Bragg wavelength is given by

$$R = \left(\frac{1 - \frac{n_s}{n_o} \left(\frac{n_L}{n_H} \right)^{2p}}{1 + \frac{n_s}{n_o} \left(\frac{n_L}{n_H} \right)^{2p}} \right)^2 \quad (2.13)$$

where the n_o and n_s are the refractive index of incident medium and substrate.

The high-reflectivity or stop band of a DBR depends on the difference in refractive index of the two constituent materials, Δn ($n_H - n_L$). The spectral width of the stop band is given by

$$\Delta\lambda_{stopband} = \frac{2\lambda_B\Delta n}{\pi m_{eff}} \quad (2.14)$$

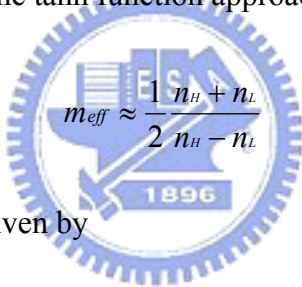
where n_{eff} is the effective refractive index of the mirror. It can be calculated by requiring the same optical path length normal to the layers for the DBR and the effective medium. The effective refractive index is then given by

$$n_{\text{eff}} = 2\left(\frac{1}{n_H} + \frac{1}{n_L}\right)^{-1} \quad (2.15)$$

The length of a cavity consisting of two metal mirrors is the physical distance between the two mirrors. For DBRs, the optical wave penetrates into the reflector by one or several quarter-wave pairs. Only a finite number out of the total number of quarter-wave pairs are effective in reflecting the optical wave. The effective number of pairs seen by the wave electric field is given by

$$m_{\text{eff}} \approx \frac{1}{2} \frac{n_H + n_L}{n_H - n_L} \tanh\left(2m \frac{n_H - n_L}{n_H + n_L}\right) \quad (2.16)$$

For very thick DBRs ($m \rightarrow \infty$) the tanh function approaches unity and one obtains



$$m_{\text{eff}} \approx \frac{1}{2} \frac{n_H + n_L}{n_H - n_L} \quad (2.17)$$

Also, the penetration depth is given by

$$L_{\text{pen}} = \frac{L_1 + L_2}{4r} \tanh(2mr) \quad (2.18)$$

where $r = (n_1 - n_2) / (n_1 + n_2)$ is the amplitude reflection coefficient.

For a large number of pairs ($m \rightarrow \infty$), the penetration depth is given by

$$L_{\text{pen}} \approx \frac{L_1 + L_2}{4r} = \frac{L_1 + L_2}{4} \frac{n_H + n_L}{n_H - n_L} \quad (2.19)$$

Comparison of Eqs. (2.17) and (2.19) yields that

$$L_{\text{pen}} = \frac{1}{2} m_{\text{eff}} (L_1 + L_2) \quad (2.20)$$

The factor of (1/2) in Eq. (2.20) is due to the fact that m_{eff} applies to effective number of periods seen by the electric field whereas L_{pen} applies to the optical power. The optical

power is equal to the square of the electric field and hence it penetrates half as far into the mirror. The effective length of a cavity consisting of two DBRs is thus given by the sum of the thickness of the center region plus the two penetration depths into the DBRs.

2.3 Fabry-Perot Resonator ^{[25-26][31-34]}

Background

The Fabry-Perot interferometer was first built and analyzed by the French physicists Fabry and Perot at the University of Marseilles about one century ago and made use of interference of light reflected many times between two coplanar lightly-silvered mirrors. It is a high resolution instrument that has been used today in precision measurement and wavelength comparisons in spectroscopy. Recent, it has come into prominence as the Fabry-Perot cavity employed in nearly all lasers. The Fabry-Perot cavities can be used to ensure precise tuning of laser frequencies.

Theory

A schematic draw of a Fabry-Perot cavity with two metallic reflectors with reflectivity R_1 and R_2 is shown in Fig 2.5. Plane waves propagating inside the cavity can interfere constructively and destructively resulting in stable (allowed) and attenuated (disallowed) optical modes, respectively. The allowed frequencies are integer multiples of the mode spacing $\Delta \nu = c/2nL_c$, where L_c is the length of the cavity, c is the velocity of light in vacuum.

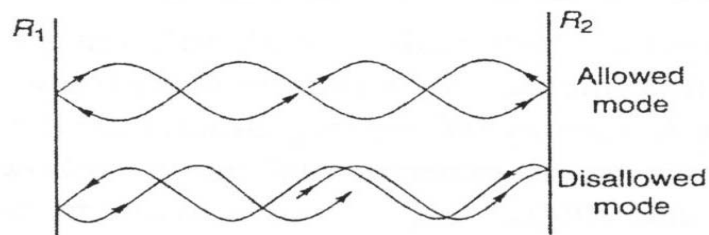


Figure 2.5 A schematic draw of a Fabry-Perot cavity with two metallic reflectors with reflectivity R_1 and R_2

For lossless reflectors, the transmittance through the two reflectors is given by $T_1 = 1-R_1$, and $T_2 = 1-R_2$. Taking into account multiple reflections inside the cavity, the transmittance through a Fabry-Perot cavity can be expressed in terms of a geometric series. The transmitted light intensity (transmittance) is then given by

$$T = \frac{T_1 T_2}{1 + R_1 R_2 - 2\sqrt{R_1 R_2} \cos 2\phi} \quad (2.21)$$

where ϕ is the phase change of the optical wave for a *single pass* between the two reflectors. The ϕ can also be expressed in term of wavelength and frequency by using

$$\phi = 2\pi \frac{nL_c}{\lambda} = 2\pi \frac{nL_c \nu}{c} \quad (2.22)$$

The maxima of the transmittance occur if the condition of constructive interference is fulfilled, that is, if $\phi = 0, 2\pi, \dots$. Insertion of these values into Eq. (2.21) yields the transmittance maxima as

$$T_{\max} = \frac{T_1 T_2}{(1 + R_1 R_2)^2} \quad (2.23)$$

For asymmetric cavities ($R_1 \neq R_2$), it is $T_{\max} < 1$. For symmetric cavities ($R_1 = R_2$), the transmittance maxima are unity, $T_{\max} = 1$. Near $\phi = 0, 2\pi, \dots$, the cosine term in Eq. (2.21) can be expanded into a power series ($\cos 2\phi \sim 1 - 2\phi^2$). One obtains

$$T = \frac{T_1 T_2}{(1 - \sqrt{R_1 R_2})^2 + \sqrt{R_1 R_2} 4\phi^2} \quad (2.24)$$

Equation (2.24) indicates that near the maxima, the transmittance can be approximated by a Lorentzian function. The transmittance T in Eq. (2.24) has a maximum at $\phi = 0$. The transmittance decreases to half of the maximum value at $\phi_{1/2} = (1 - \sqrt{R_1 R_2}) / (4\sqrt{R_1 R_2})^{1/2}$. For high values of R_1 and R_2 (i.e., $R_1 \sim 1$ and $R_2 \sim 1$), it is $\phi_{1/2} = (1/2)(1 - \sqrt{R_1 R_2})$.

2.4 The Finesse and the Quality Factor of Resonant Cavity ^{[25-26][31-34]}

Since the theory of Fabry-Perot cavity has been explained, we can talk about the finesse and the quality factor of resonant cavity. The cavity finesse, F , is defined as the ratio of the transmittance peak separation ($\Delta\phi$) to the transmittance full-width at half-maximum ($\delta\phi$):

$$F = \frac{\Delta\phi}{\delta\phi} = \frac{\pi}{2\phi_{1/2}} = \frac{\pi}{1 - \sqrt{R_1 R_2}} \quad (2.25)$$

Figure 2.6 shows the transmission pattern of a Fabry-Perot cavity in frequency domain. The finesse of the cavity in the frequency is then given by $F = \nu_{FSR} / \Delta \nu$.

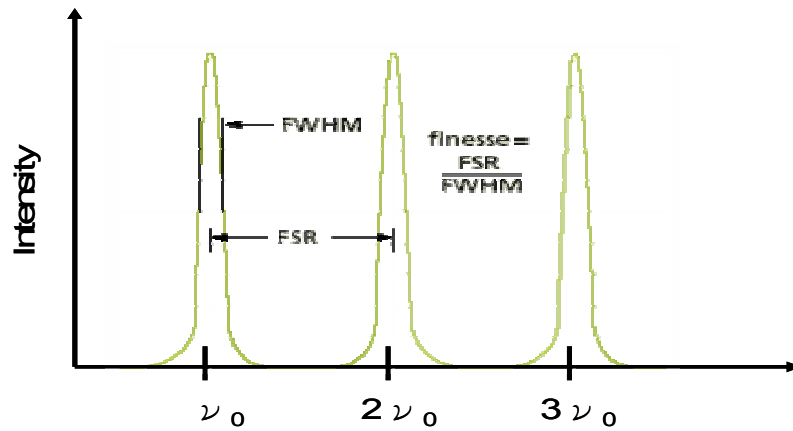


Figure 2.6 The transmission pattern of a Fabry-Perot cavity in frequency domain.

The cavity quality factor Q is frequently used and is defined as the ratio of the transmittance peak frequency (ϕ) to the peak width ($\delta \phi$):

$$Q = \frac{\phi}{\delta \phi} = \frac{2nL_c}{\lambda} \frac{\pi}{1 - \sqrt{R_1 R_2}} \quad (2.26)$$

Besides the quality factor Q is also equal to $\lambda / \delta \lambda$, where $\delta \lambda$ is the narrow emission linewidth around λ .

$$Q = \frac{\lambda}{\delta \lambda} \quad (2.27)$$

2.5 Operation Mechanism of VCSEL ^{[25-27][35-38]}

The operation of a VCSEL, like any other diode lasers, can be understood by observing the flow of carriers into its active region, the generation of photons due to the recombination of some of these carriers, and the transmission of some of these photons out of the optical cavity. These dynamics can be described by a set of rate equations, one for the carriers and one for the photons in each of the optical modes. In fact, the construction of such rate equations provides a clear definition of the basic laser parameters that we will need in describing the terminal characteristic of the VCSEL.

Carrier density rate equation

The carrier density in the active region is governed by a dynamic process. In fact, we can compare the process of establishing a certain steady-state carrier density in the active region to that of establishing a certain water level in a reservoir which is being simultaneously filled and drained. This is shown schematically in Fig. 2.7. As we proceed, the various filling (generation) and drain (recombination) terms illustrated will be defined. The current leakage illustrated in Fig. 2.7 contributes to reducing η_i and is created by possible shunt paths around the active region. The carrier leakage, R_l , is due to carriers “splashing” out of the active region (by thermionic emission or lateral diffusion if no lateral confinement exists) before recombining. Thus, this leakage contributes to a loss of carriers in the active region that could otherwise be used to generate light.

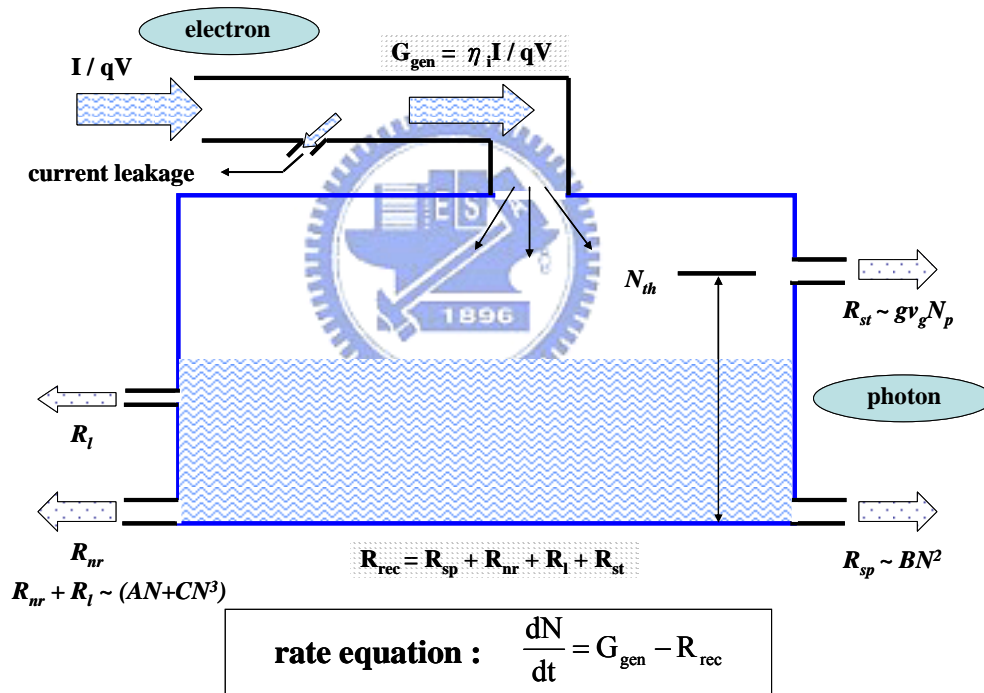


Figure 2.7 Reservoir with continuous supply and leakage as an analog to a DH active region with current injection for carrier generation and radiative and nonradiative recombination.

For the DH active region, the injected current provides a generation term, and various radiative and nonradiative recombination process as well as carrier leakage provide recombination terms. Thus, we can write the carrier density rate equation,

$$\frac{dN}{dt} = G_{gen} - R_{rec} \quad (2.28)$$

where N is the carrier density (electron density), G_{gen} is the rate of injected electrons and R_{rec} is the ratio of recombining electrons per unit volume in the active region. Since there are $\eta_i I/q$ electrons per second being injected into the active region, $G_{gen} = \frac{\eta_i I}{qV}$, where V is the volume of the active region. The recombination process is complicated and several mechanisms must be considered. Such as, spontaneous recombination rate, $R_{sp} \sim BN^2$, nonradiative recombination rate, R_{nr} , carrier leakage rate, R_l , ($R_{nr} + R_l = AN + CN^3$), and stimulated recombination rate, R_{st} . Thus we can write $R_{rec} = R_{sp} + R_{nr} + R_l + R_{st}$. Besides, $N/\tau \equiv R_{sp} + R_{nr} + R_l$, where τ is the carrier lifetime. Therefore, the carrier density rate equation could be expressed as

$$\left(\begin{array}{l} \text{carrier density} \\ \text{rate equation} \end{array} \right) \quad \frac{dN}{dt} = \frac{\eta_i I}{qV} - \frac{N}{\tau} - R_{st} \quad (2.29)$$

Photon density rate equation

Now, we describe a rate equation for the *photon density*, N_p , which includes the photon generation and loss terms. The photon generation process includes spontaneous recombination (R_{sp}) and stimulated recombination (R_{st}), and the main photon generation term of laser above threshold is R_{st} . Every time an electron-hole pairs is stimulated to recombine, another photon is generated. Since, the cavity volume occupied by photons, V_p , is usually larger than the active region volume occupied by electrons, V , the photon density generation rate will be $[V/V_p]R_{st}$ not just R_{st} . This electron-photon overlap factor, V/V_p , is generally referred to as the *confinement factor*, Γ . Sometimes it is convenient to introduce an effective thickness (d_{eff}), width (w_{eff}), and length (L_{eff}) that contains the photons. That is, $V_p = d_{eff} w_{eff} L_{eff}$. Then, if the active region has dimensions, d , w , and L_a , the confinement factor can be expressed as, $\Gamma = \Gamma_x \Gamma_y \Gamma_z$, where $\Gamma_x = d/d_{eff}$, $\Gamma_y = w/w_{eff}$, $\Gamma_z = L_a/L_{eff}$. Photon loss occurs within the cavity due to optical absorption and scattering out of the mode, and it also occurs at the output coupling mirror where a portion of the resonant mode is usually couple to some output medium. These net losses can be characterized by a *photon (or cavity) lifetime*, τ_p . Hence, the photon density rate equation takes the form

$$\left(\begin{array}{l} \text{photon density} \\ \text{rate equation} \end{array} \right) \quad \frac{dN_p}{dt} = \Gamma R_{st} + \Gamma \beta_{sp} R_{sp} - \frac{N_p}{\tau_p} \quad (2.30)$$

where β_{sp} is the *spontaneous emission factor*. As to R_{st} , it represents the photon-stimulated net electron-hole recombination which generates more photons. This is a **gain** process for

photons. It is given by

$$\left(\frac{dN_p}{dt} \right)_{gen} = R_{st} = \frac{\Delta N_p}{\Delta t} = v_g \mathbf{g} N_p \quad (2.30)$$

where v_g is the group velocity and \mathbf{g} is the gain per unit length.

Now, we rewrite the carrier and photon density rate equations

$$\left(\begin{array}{l} \text{carrier density} \\ \text{rate equation} \end{array} \right) \quad \frac{dN}{dt} = \frac{\eta_i I}{qV} - \frac{N}{\tau} - v_g \mathbf{g} N_p \quad (2.31)$$

$$\left(\begin{array}{l} \text{photon density} \\ \text{rate equation} \end{array} \right) \quad \frac{dN_p}{dt} = \Gamma v_g \mathbf{g} N_p + \Gamma \beta_{sp} R_{sp} - \frac{N_p}{\tau_p} \quad (2.32)$$

Threshold gain

In order for a mode of the laser to reach threshold, the gain in the active section must be increased to the point when all the propagation and mirror losses are compensated. As illustrated in Fig. 2.8, most laser cavities can be divided into two general sections: an active section of length L_a and a passive section of length L_p . The threshold gain is given by

$$\Gamma \mathbf{g}_{th} = \alpha_i + \frac{1}{2L} \ln \left(\frac{1}{R_1 R_2} \right) \quad (2.33)$$

where α_i is the average internal loss which is defined by $(\alpha_{ia} L_a + \alpha_{ip} L_p)/L$, and R_1 and R_2 is the reflectivity of top and bottom mirror of the laser cavity, respectively. For convenience the mirror loss term is sometimes abbreviated as, $\alpha_m \equiv (1/2L) \ln(1/R_1 R_2)$. Noting that the cavity life time (photon decay rate) is given by the optical loss in the cavity, $1/\tau_p = 1/\tau_i + 1/\tau_m = v_g(\alpha_i + \alpha_m)$. Thus, the threshold gain in the steady state can be expressed with following equation

$$\Gamma \mathbf{g}_{th} = \alpha_i + \alpha_m = \frac{1}{v_g \tau_p} = \alpha_i + \frac{1}{2L} \ln \left(\frac{1}{R_1 R_2} \right) \quad (2.34)$$

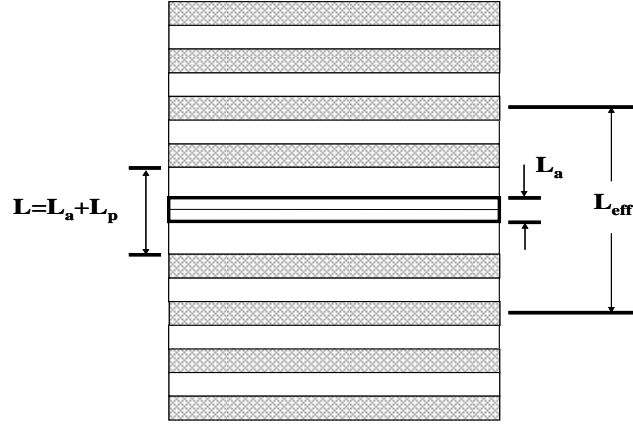


Figure 2.8 Schematic diagram of VCSEL

Output power versus driving current

The characteristic of output power versus driving current (L-I characteristic) in a laser diode can be realized by using the rate equation Eq. (2.31) and (2.32). Consider the below threshold (almost threshold) steady-state ($dN/dt = 0$) carrier rate equation, the Eq. (2.31) is

given by $\frac{\eta_i I_{th}}{qV} = (R_{sp} + R_{nr} + R_l)_{th} = \frac{N_{th}}{\tau}$. While the driving current is above the threshold ($I > I_{th}$), the carrier rate equation will be

$$\left(\begin{array}{l} \text{above threshold} \\ \text{carrier density} \\ \text{rate equation} \end{array} \right) \quad \frac{dN}{dt} = \eta_i \frac{(I - I_{th})}{qV} - v_g \mathbf{g} N_p \quad (2.35)$$

From Eq. (2.35), the steady-state photon density above threshold where $\mathbf{g} = \mathbf{g}_{th}$ can be calculated as

$$\left(\begin{array}{l} \text{steady state} \\ \text{photon density} \end{array} \right) \quad N_p = \frac{\eta_i (I - I_{th})}{qv_g \mathbf{g}_{th} V} \quad (2.36)$$

The optical energy stored in the cavity, E_{os} , is constructed by multiplying the photon density, N_p , by the energy per photon, $h\nu$, and the cavity volume, V_p . That is $E_{os} = N_p h\nu V_p$. Then, we multiple this by the energy loss rate through the mirrors, $v_g \alpha_m = 1/\tau_m$, to get the optical power output from the mirrors, $P_0 = v_g \alpha_m N_p h\nu V_p$. By using Eq. (2.34) and (2.36), and $\Gamma = V/V_p$, we can write the output power as the following equation

[output power]
$$P_o = \eta_i \left(\frac{\alpha_m}{\alpha_i + \alpha_m} \right) \frac{h\nu}{q} (I - I_{th}) \quad (2.37)$$

Now, by defining $\eta_d = \frac{\eta_i \alpha_m}{\alpha_i \alpha_m}$, the Eq. (2.37) can be simplified as

$$P_o = \eta_d \frac{h\nu}{q} (I - I_{th}) \quad (I > I_{th}) \quad (2.38)$$

Thus, the η_d can be expressed as

[differential quantum efficiency]
$$\eta_d = \left[\frac{q}{h\nu} \right] \frac{dP_o}{dI} \quad (I > I_{th}) \quad (2.39)$$

In fact, η_d is the *differential quantum efficiency*, defined as number of photons out per electron. Besides, dP_o/dI is defined as the *slope efficiency*, S_d , equal to the ratio of output power and injection current. Figure 2.9 shows the illustration of output power vs. current for a diode laser. below threshold only spontaneous emission is important; above threshold the stimulated emission power increase linearly with the injection current, while the spontaneous emission is clamped at its threshold value.

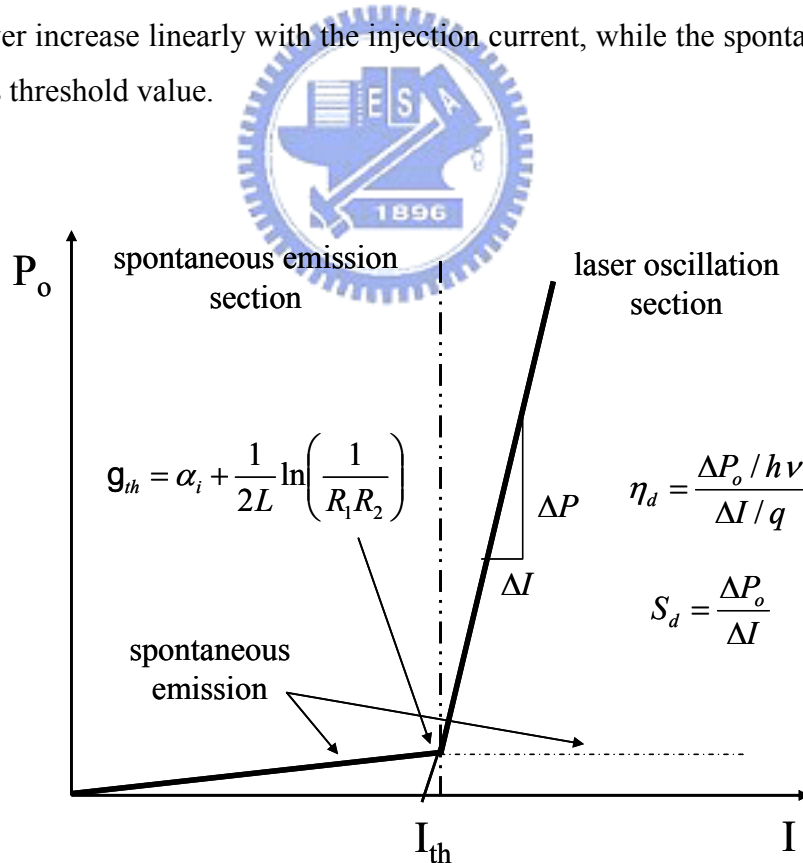


Figure 2.9 Illustration of output power vs. current for a diode laser.

Temperature dependent threshold current

The threshold current I_{th} is relative to three temperature dependent factors: N_{tr} , g_o , and α_i , where $N_{tr} \propto T$, $g_o \propto 1/T$, and $\alpha_i \propto T$. The transparency carrier density is increased and the gain parameter is reduced because injected carriers spread over a wider range in energy with high temperature. The increased internal loss results from the required higher carrier densities for threshold. Since, both the gain and the internal loss variations result in an exponential temperature dependence of the threshold current, while the linear dependence of the transparency carrier density is not significant over small temperature ranges. Thus, the threshold current can be approximately modeled by

$$I_{th(T)} = I_{th(T')} \exp\left(\frac{T - T'}{T_o}\right) \quad (2.40)$$

where $I_{th(T)}$ is the threshold at T , and T_o is called the characteristic temperature. Both temperatures are given in degrees Kelvin, K. The larger the characteristic temperature is, the smaller the temperature dependence.

